Heterogeneous Chemistry of Organic Acids on Soot Surfaces

Nicholas P. Levitt,[†] Renyi Zhang,*[,†] Huaxin Xue,[‡] and Jianmin Chen[‡]

Department of Atmospheric Sciences, Texas A&M University, College Station, Texas 77843, and Department of Environmental Science and Engineering, Fudan University, Shanghai 200433, People's Republic of China

Received: January 3, 2007; In Final Form: February 22, 2007

We have investigated the heterogeneous interaction between a number of carboxylic acids and soot generated from different fuel sources and formation mechanisms. A low-pressure fast flow reactor in conjunction with ion drift−chemical ionization mass spectrometry detection was employed to study uptake of monocarboxylic (benzoic, oleic, and steric) and dicarboxylic (glutaric, maleic, oxalic, and phthalic) acids on deposited soot surfaces formed by combustion of methane, propane, and kerosene. Most acids exhibited irreversible uptake on the soot surfaces and the uptake coefficient was measured in the range of 9×10^{-4} to 1×10^{-1} estimated based on the geometric surface areas. Brunauer, Emmett, and Teller surface areas of the deposited soot surfaces were measured and the soot bulk and surface chemical compositions were evaluated with Fourier transform infrared spectroscopy and attenuated total reflection spectroscopy. Plausible uptake mechanisms were discussed on the basis of the measured soot physiochemical properties by comparing the mono and dicarboxylic acids.

1. Introduction

Aerosols play a vital role in many atmospheric processes. They have been shown to directly affect radiation balance through reflection or scattering of visible light and absorbing visible and infrared energy.[1] Aerosols are also capable of promoting cloud formation by acting as cloud condensation nuclei (CCN) and thus indirectly impact the global radiation balance.[2] These phenomena can cause aerosols to impact global climate on a longer time scale.[3] Aerosols have also been shown to be detrimental to human health, air quality, and visibility.[4] Soot, a form of black carbon, is one common type of atmospheric aerosols that is of special concern because of the uncertainty surrounding its involvement in direct and indirect climate forcing. Soot is the result of incomplete hydrocarbon combustion and has a been estimated to have a global emission rate of 8−24 Tg yr^{-1}.[5,6] Soot aerosols are ubiquitous in the atmosphere. Schultz reported black carbon as being ∼ 20% of the total particulate matter in the 3−48 μm range in Berlin.[7] Gray et al. found 14.9% of all fine aerosols are elemental carbon in Los Angeles.[8] Kaneyasu and Murayama measured black carbon concentrations over 150 ng C m^{-3} above the central Pacific Ocean.[9] The fate of soot depends on its level of aging in the atmosphere. Soot that has been oxidized or coated may interact with water in the atmosphere and follow wet deposition pathways rather than dry deposition that its hydrophobic nature would necessitate. One class of organic species relevant to the atmospheric aging of soot is organic acids. Organic acids are produced from oxidation of volatile organic compounds (VOCs) as well as from biomass and fuel burning.[10−13] Larger fatty acids can enter the atmosphere after being shed by plant and animal material or through anthropogenic processes such as grilling and frying.[14−20]

A wide variety of experimentation and field monitoring has been conducted to understand the role of soot in the atmosphere. In addition to the annual emission rate and concentrations, other physical properties of soot have been investigated. Soot formation occurs after pyrolysis of hydrocarbons where ionic carbon atoms or molecule fragments recombine to form aromatic and polyaromatic structures. Mansurov explained in a recent review[21] that these conjugated systems continue to assemble in continuous graphite-like sheets until the structures are large enough to condense. After particles are formed, they continue to grow through surface deposition and finally coagulation and aggregation. Soot particles can grow up to a few micrometers in length.[22] The resulting soot particles possess large porosities and significant internal surface areas. Passages between pores tend to resemble nanotubes with micro and mesopores forming among spherical elementary particles.[23] Soot formation is critically sensitive to the conditions in which it is produced. Temperature, pressure, air mixing ratio, pyrolysis initiation method, and other factors can change the resulting soot circumstances. Elemental makeup of soot is between 80 and 100% carbon depending on the fuel with the balance consisting of mainly hydrogen and oxygen with the possibility of some nitrogen and sulfur.[24,25] Soot has a tremendous ability to absorb solar and terrestrial radiation, but factors such as coating by organic and inorganic compounds and the resulting changes in absorption cross section can dramatically alter the absorption and single scattering albedo of soot.[26,27] The understanding of these properties and interaction consequences is crucial for modeling of aerosol microphysics and cloud/climate interaction.

Much attention has been paid to soot aging and interaction with atmospheric gas-phase species recently.[23,28−31] These studies have focused on the aging of soot as it relates to the CCN forming potential[32] and alteration of optical properties[33] as well as the possible role that soot could play in ice nucleation[34] or acting as a substrate for atmospheric reduction−oxidation reactions.[35] Uptake coefficients on soot have been measured for ozone,[36,37] water,[25,38] sulfuric acid,[32] nitric acid,[37,39−41] nitrogen dioxide,[40−43] and nitrogen pentoxide.[37] Other studies have focused on organic uptake by other carbonaceous solid matter; these studies investigated polyaromatic

* Author to whom correspondence should be addressed. E-mail: zhang@ariel.met.tamu.edu. Tel: 979-845-7656. Fax: 979-862-4466.
[†] Texas A&M University.
[‡] Fudan University.

10.1021/jp0700480 CCC: $37.00
Published on Web 05/12/2007

TABLE 1: Summary of Measurements of Uptake Coefficients of Monocarboxylic Acids on Soot[a]

	steric acid			oleic acid			benzoic acid		
	exp no	γ (10^{-2})	dev (10^{-2})	exp no	γ (10^{-2})	dev (10^{-2})	exp no	γ (10^{-2})	dev (10^{-2})
					methane soot				
	1	0.98	0.45	1	0.95	0.38	1	0.21	0.07
	2	0.7	0.27	2	0.59	0.18	2	0.17	0.03
	3	0.53	0.26	3	0.48	0.08	3	0.16	0.04
	4	0.44	0.16	4	0.46	0.02	4	0.16	0.04
	5	0.34	0.12	5	0.48	0.04	5	0.16	0.04
	6	0.28	0.07	6	0.44	0.03	6	0.14	0.03
	mass	8 ± 5 mg		mass	8 ± 6 mg		mass	9 ± 5 mg	
					propane soot				
Type B	1	3.43	0.99	1	5.84	0.86	1	n/a	n/a
	2	2.32	1.19	2	5.25	1.26	2	n/a	n/a
	3	1.43	0.75	3	4.13	1.47	3	n/a	n/a
	4	0.98	0.5	4	3.51	1.3	4	n/a	n/a
	5	0.63	0.32	5	3.18	1.06	5	n/a	n/a
	6	0.43	0.26	6	3.22	0.93	6	n/a	n/a
	mass	3 ± 1 mg		mass	12 ± 1 mg		mass	n/a	n/a
Type A	1	3.54	1.11	1	10.05	1.27	1	0.98	0.36
	2	2.67	0.81	2	8.75	1.03	2	0.94	0.49
	3	2.58	0.77	3	8.03	1.37	3	0.55	0.21
	4	2.12	0.7	4	6.91	2.06	4	0.43	0.12
	5	1.58	0.4	5	5.91	1.25	5	0.35	0.07
	6	1.23	0.39	6	5.18	0.68	6	0.3	0.09
	mass	25 ± 14 mg		mass	20 ± 10 mg		mass	31 ± 8 mg	
					kerosene soot				
Type B	1	5.03	1.23	1	4.44	1.18	1	1.74	0.37
	2	4.1	1.1	2	3.61	1.52	2	0.95	0.16
	3	3.47	1.13	3	2.75	1.43	3	0.79	0.34
	4	3.06	1.11	4	3.25	1.88	4	0.77	0.29
	5	3.01	0.95	5	2.91	2.05	5	0.47	0.2
	6	2.72	0.96	6	2.56	1.97	n/a	n/a	n/a
	mass	36 ± 18 mg		mass	13 ± 14 mg		mass	6 ± 1 mg	
Type A	1	5.36	2.05	1	n/a	n/a	1	1.33	0.83
	2	4.9	2.54	2	n/a	n/a	2	0.79	0.71
	3	3.59	1.68	3	n/a	n/a	3	0.57	0.39
	4	3.16	2	4	n/a	n/a	4	0.59	0.44
	5	2.74	1.62	5	n/a	n/a	5	0.51	0.3
	6	1.88	1.2	6	n/a	n/a	6	0.63	0.49
	mass	41 ± 11 mg		mass	n/a	n/a	mass	42 ± 27 mg	

[a] At least three uptake sequences were used to average uptake values and masses. Error corresponds to second standard deviation (σ^2).

TABLE 2: Summary of Measurements of Uptake Cofficients of Dicarboxylic Acid on Soot[a]

				propane		kerosene	
acid	C[b]	DB[c]	methane γ (10^{-2})	Type B γ (10^{-2})	Type A γ (10^{-2})	Type B γ (10^{-2})	Type A γ (10^{-2})
oxalic	2	0	0.09 ± 0.01	none	0.17 ± 0.02	0.18 ± 0.10	0.18 ± 0.05
maleic	4	1	reversible	none	*d*	reversible	reversible
glutaric	5	0	0.59 ± 0.12	reversible	0.37 ± 0.12	0.42 ± 0.12	0.46 ± 0.06
phthalic	aromatic		0.76 ± 0.26	0.38 ± 0.07	0.65 ± 0.24	0.57 ± 0.01	0.77 ± 0.47

[a] The uptake coefficients represent averages of at least two experiments. Error corresponds to second standard deviation (σ^2). [b]Number of carbon atoms in molecule. [c]Number of double bonds in molecule. [d]Showing both reversible and irreversible behaviors.

hydrocarbon (PAH) uptake on coal fly ash,[44] PAH sorption by carbon nanomaterials,[45] and benzene derivatives and cyclohexane on wood charcoals.[46] The uptake experiments reported a range of coefficients varying by several orders of magnitude. Generally, as soot became aged, the tendency for gas-phase species to adsorb to the surface decreased. Gas-phase concentrations and soot types also played a role in heterogeneous partitioning, but the key factor in determining the uptake appeared to be the adsorbate. In addition, an optical study has been reported for an organic acid and soot interaction.[47] Heterogeneous reactions on soot particles can have significant impacts on chemical transformation of trace species[48] and UV radiation reduction,[49] hence influencing the air quality.[50] A better knowledge of the interaction between soot particles and organic acids is necessary to assess the atmospheric lifetime of soot aerosols and their direct and indirect effects on climate.

In this work, we have studied the interaction between several monocarboxylic and dicarboxylic acids and soot formed by combustion of methane, propane, and kerosene. Soot was deposited by either allowing the flame to come into contact with the deposition surface or by positioning the deposition substrate well above the flame level. Monocarboxylic acids used in this study were benzoic, steric, and oleic, and dicarboxylic acids included oxalic, maleic, glutaric, and phthalic. For monocarboxylic acids that exhibited irreversible loss on soot, the uptake coefficient was measured several times sequentially to evaluate

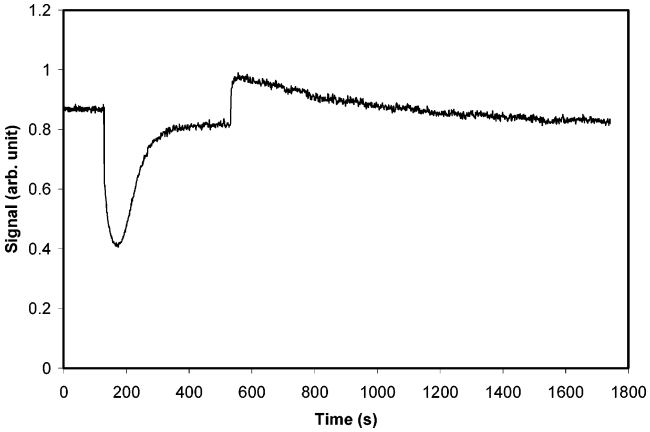

Figure 1. Temporal profile of maleic acid with temporary exposure to 58 mg of Type B kerosene soot over a 20 cm length. The gas-phase concentration of maleic acid was estimated to be 1×10^{11} molecules cm^{-3}. The exposure was terminated after 500 s.

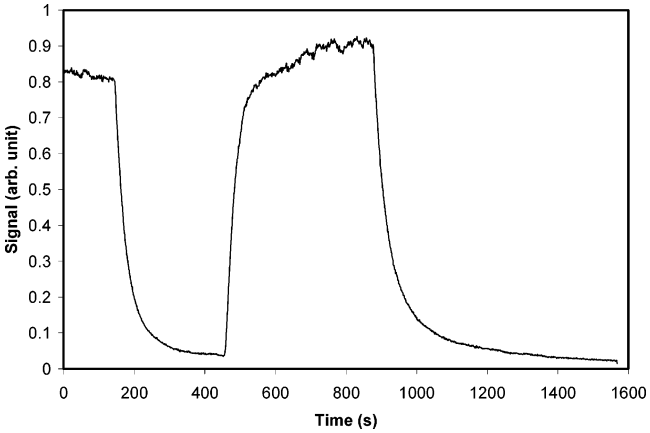

Figure 2. Temporal profile of phthalic acid with temporary exposure to 35 mg of methane soot over a 20 cm length. The gas-phase concentration of phthalic acid was estimated to be 5×10^{10} molecules cm^{-3}. The phthalic acid flow was terminated after 900 s.

the aging affect on uptake. The physical and chemical properties of the soot samples were investigated to help explain differences in the uptake for different organic acid/soot combinations. Brunauer, Emmett, and Teller (BET) isotherms were performed to assess soot surface areas, and Fourier transform infrared (FTIR) spectroscopy and attenuated total reflection (ATR) spectroscopy were utilized to examine functional groups inside and on the surface of soot.

2. Experimental Section

2.1. Uptake Measurements. The uptake measurements were performed using a low-pressure laminar flow reactor in conjunction with ion drift−chemical ionization mass spectrometry (ID-CIMS) detection, similar to the work described by us previously.[48−50] A Pyrex reactor of 70 cm in length with an internal radius of 1 cm was used. Within the reactor, a smaller glass tube (20 cm long with an internal radius of 0.8 cm) with soot coating on the inside walls was placed.

Benzoic acid (Fisher Scientific, 99.5%), glutaric acid (Sigma, 99%), maleic acid (Sigma-Aldrich, 99%), oleic acid (Sigma, ∼99%), oxalic acid (Aldrich, 98%), phthalic acid (Sigma-Aldrich, 99.5%), and steric acid (Sigma-Aldrich, 95%) were used as received without further purification. A bubbler containing the acid was placed in a temperature bath to regulate its concentration in the flow reactor. For benzoic acid, a room-temperature bath was used, and for other organic acids the bath

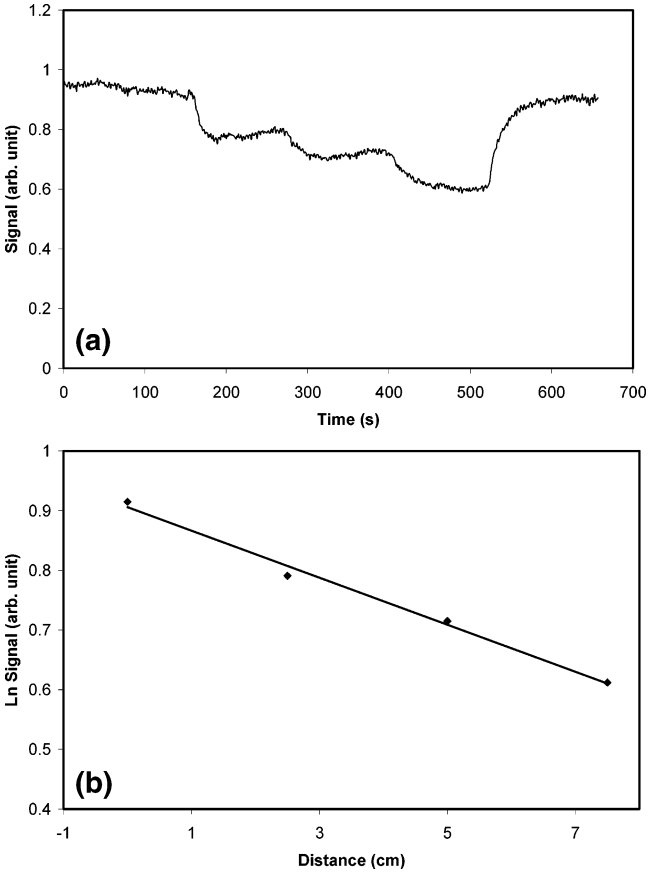

Figure 3. (a) Temporal profile of benzoic acid with stepwise exposure in 2.5 cm increments to 15 mg of methane soot over a 7.5 cm length. Experimental conditions are $T = 296$ K, $P = 0.29$ Torr, $u = 344$ cm s^{-1}, and the gas-phase concentration of benzoic acid was estimated to be 1×10^{13} molecules cm^{-3}. The injector was returned to its original position after 500 s. (b) Intensity of acid signal as a function of injector distance. Solid diamonds identify benzoic acid data taken from the experiment described in Figure 3a.

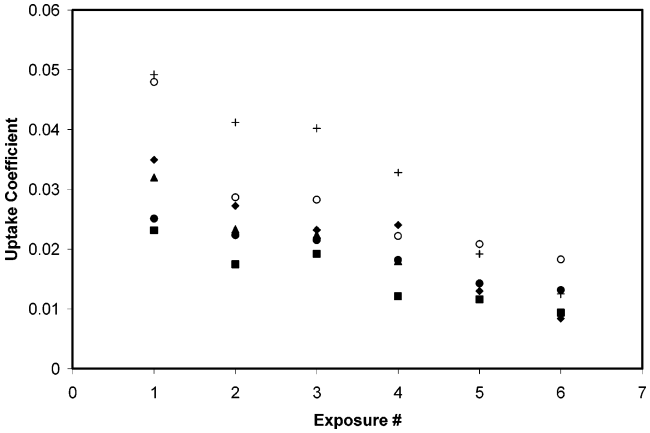

Figure 4. Comparison of uptake coefficients as a function of exposure number for steric acid uptake on different amounts of Type A propane soot. The gas-phase concentration of steric acid was estimated to be 5×10^{11} molecules cm^{-3}. Crosses, open circles, and diamonds represent masses 13.3, 18.0, and 47.7 mg respectively, while triangles, closed circles, and squares represent masses 21.7, 12.2, and 36.8 mg, respectively.

temperature was maintained between 50 and 100 °C. The acid purity was checked by ID-CIMS. The acid vapor was introduced into the flow reactor through a movable injector. The vapor concentrations of the organic acids in the flow reactor were estimated to be on the order of 10^{-4} to 10^{-6} Torr. Little or no

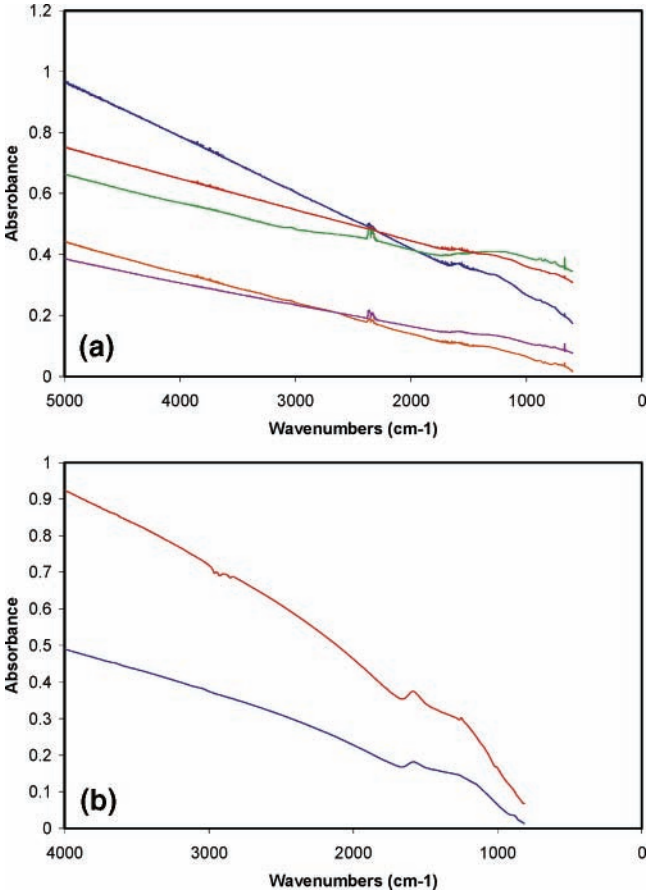

Figure 5. (a) IR spectra of propane soot deposited on ZnSe crystal plates. The top three spectra are Type A samples and the bottom two are Type B. Spectra are shifted for clarity. (b) ATR spectra of kerosene soot corrected for comparison to IR spectra and shifted for clarity. The top spectrum is of Type B soot and the bottom is of Type A soot.

vapor pressure information is available for most of the organic acids used in this study. The vapor concentrations of the organic acids were mainly estimated on the basis of extrapolation from very few results available in literature. For several compounds, we could not identify a literature value, and for those cases we estimated the vapor concentrations on the basis of measured signal intensities compared to a known concentration of a similar compound.

All carrier flows were monitored with calibrated electronic mass flow meters (Millipore Tylan 260 Series). The flow reactor was operated under the laminar flow conditions (i.e., the Reynold number $\mathrm{Re} = 2au\rho/\mu < 2000$, where a is the internal radius of the flow reactor in cm, ρ is the density of the gas in g cm^{-3}, u is the flow velocity in cm s^{-1}, and μ is the absolute viscosity of the gas) with a pressure of about 0.35 Torr and typical flow velocities of 500−800 cm s^{-1}.

Soot was deposited on the sample tube for approximately an hour for a typical experiment. For methane and propane, a commercial burner was used, and a commercial alcohol burner was used to produce the kerosene flame. During the coating process, the flame was adjusted by altering the amount of fuel available to produce a "sooting" flame to speed up the deposition process. The soot surfaces were produced in two different manners. First, the flame was allowed to exist inside the tube so that the fire came in contact with the wall due to the natural motion of the flame. The second process had the tube well above the tip of the flame so that the tube walls were never directly exposed to the flame. In the present work, the first method is referred to as Type A while the second is referred to as Type B. The Type A method was also referred to as "activated" soot by Aubin and Abbatt in the investigation of nitric acid adsorption to hexane soot.[35] For the methane flame, combustion was sufficiently effective that soot was not deposited unless the Type A method was employed. For this reason, only Type A soot was used for methane experiments. The mass of soot deposited in the tube varied with the fuel source and with the two methods. The amounts of soot ranged from a few milligrams to 200 milligrams. The soot tube was replaced with a fresh sample for each new experiment and the amount of soot on the tube was measured after each experiment. The mass of soot remained unchanged before and after the experiments.

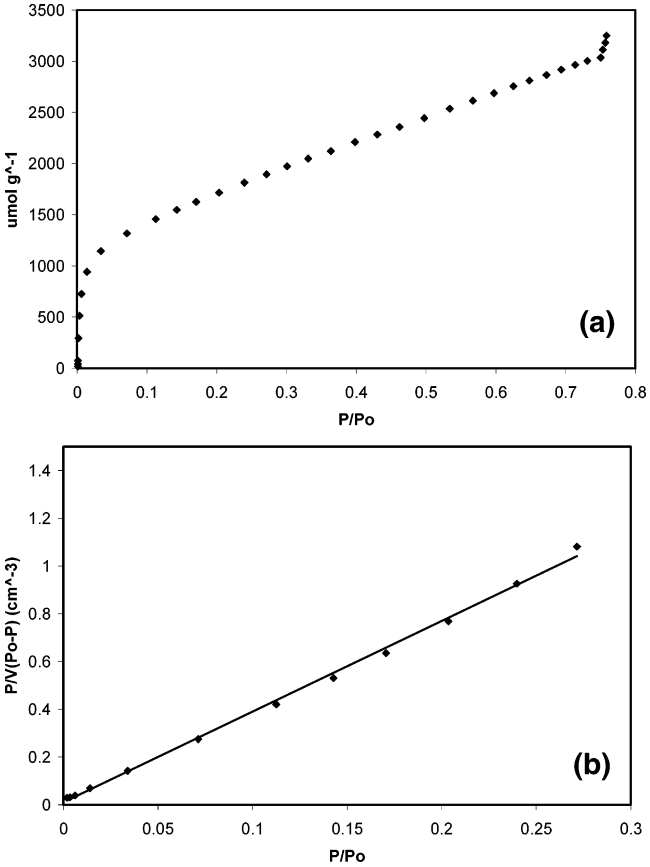

Figure 6. (a) Adsorption isotherm of Kr on 0.0144 g of Type B kerosene soot at 77.5 K. (b) BET plot of $P/V(P_0 - P)$ against P/P_0.

Details of the ID−CIMS instrumentation have been described previously.[51−53] Briefly, the proton-transfer reaction with H_3O^+ was used

$$H_3O^+ + X \rightarrow XH^+ + H_2O \qquad (1)$$

where X and XH^+ denote the organic acid or its fragment and the corresponding protonated form, respectively. Maleic acid, oleic acid, phthalic acid, and steric acid were monitored at their protonated fragmentation peaks ($m/z = 99$ for maleic acid, 169 for oleic acid, 149 for phthalic acid, and 145 for steric acid) for high-detection sensitivity. The intensity of the fragment peak was observed to be linearly proportional to that of its parent acid flow tube concentration. Benzoic acid, glutaric acid, and oxalic acid were monitored at their protonated peaks ($m/z =$ 123 for benzoic acid, 133 for glutaric acid, and 91 for oxalic acid).

The interaction between soot and organic acids were assessed by exposing a length of the soot tube to the flow of organic

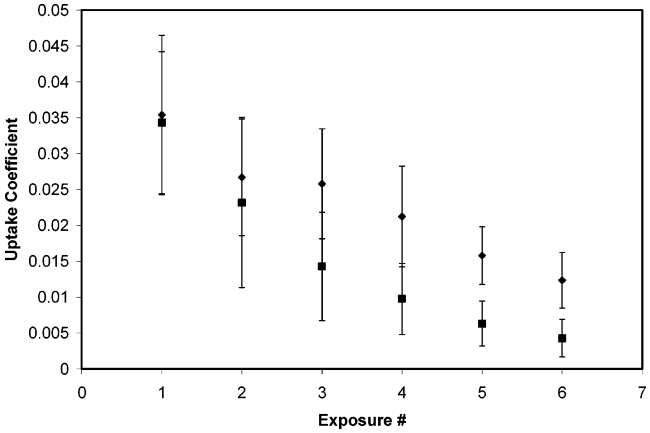

Figure 7. Uptake coefficient as a function of exposure number for steric acid uptake on propane soot. Solid squares identify Type A data taken from Table 2, and solid diamonds are Type B soot data taken from the same table. Error bars represent the standard deviation also given in Table 1.

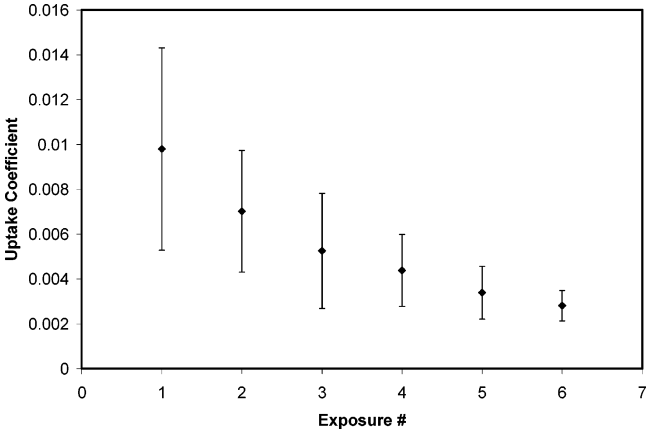

Figure 8. Uptake coefficient values are displayed as a function of exposure number for steric acid uptake on methane soot. The uncertainty of the measurements decreases with progressive exposures.

acid vapor when retracting the moveable injector to a position upstream of the soot tube. In the cases of irreversible loss, the signal dropped to a lower level and did not increase significantly on the time scale of the experiment. The uptake coefficient (γ) was determined by monitoring the signal of the organic acid as it was exposed to the soot. The uptake coefficient represents the ratio of gas-surface collisions that result in loss of organics to the surface to the sum of all gas-surface collisions. To calculate the uptake coefficient, the first-order rate constant (k) was measured from the signal loss[54−56]

$$\gamma = \frac{2rk}{\omega + rk} \tag{2}$$

where r is the radius of the flow reactor and ω is the mean thermal speed. The geometric inner surface area of the soot tube was used in the uptake coefficient calculations. Gas-phase diffusion correction was accomplished according to Brown,[57] allowing for description of radial organic acid gradients in the reaction chamber due to significant reactive wall loss and determination of the observed first-order reaction rate constant (k_{obs}). The gas-phase diffusion coefficients were estimated by the method described by Fuller et al.[58] with the improvements suggested by Marrero and Luecke.[59] The values used for steric acid, oleic acid, and benzoic acid were 102.8, 103.8, and 193.9 Torr cm^2 s^{-1}, respectively. The gas-phase diffusion coefficients of dicarboxylic acid were estimated to be 240.9, 178.9, and 167.111 Torr cm^2 s^{-1} for oxalic, glutaric, and phthalic acid, respectively. For steric acid, the uptake coefficient was underestimated by 18 to 45% without the Brown correction for uptake coefficients up to 0.05, and for an uptake coefficient of 0.065 the corrected value was 57% higher. For oleic acid, the correction was in the range of 17−40% for the uptake coefficients between 0.016 and 0.07. The highest uptake coefficients (∼0.1) had a deviation of 50%. For benzoic acid, the correction was 17−40% for the uptake coefficients of up to 0.008 but was 48% for the uptake coefficient of 0.017. For most dicarboxylic acids, the corrections were around 30%.

2.2. Soot Characterization by FTIR and ATR Spectroscopy. The chemical composition of the soot surface is of special interest in this study. To describe and attribute organic acid/surface interaction, it is necessary to understand the structure at the soot surface and available functional groups. To investigate this property, we made use of FTIR and ATR spectroscopy on deposited surfaces.

Soot was deposited on a ZnSe crystal plate in one of the two manners described in the previous section for Type B or Type A soot. The coating was fairly thin (∼1 mg) to prevent total absorbance of IR light. A Nicolet Magna 560 spectrometer with mercury cadmium telluride (MCT) detector was used to measure spectra at 2 cm^{-1} resolution for the FTIR investigations. An average of 64 scans was used to collect spectra in a typical wavenumber range from 5000 to 750 cm^{-1}.

The ATR-FTIR instrument used in this study was a Perkin-Elmer Spectrum 100 employing a mid-infrared (MIR) TGS detector. The crystal type used was ZnSe and had the dimensions of 1 cm × 5 cm and a penetration depth of 0.5−5 μ. ATR spectra were corrected for comparison to FTIR spectra after averaging a collection of 20 scans at a resolution of 4 cm^{-1} over the typical wavenumber range from 4000 to 750 cm^{-1}. Soot was deposited on a single side of commercial aluminum foil in the manner described above in order to test Type A or B soot. The foil was cut to fit into the depression above the ATR crystal and to allow efficient contact between the soot and crystal surface. The crystal was cleaned of all soot between experiments, and blank samples confirmed the absence of absorbing material on the surface.

2.3. BET Surface Area Measurements. We performed surface area measurements of the deposited soot employing theBET method.[60] Soot surface areas for *n*-hexane have been found to be 88−372 times larger than the geometric surface area occupied by the soot.[35] For this reaso, we have employed this technique to probe the relationship between Types A and B and the resulting surface area.

The BET procedure involved using a specified gas to create an adsorption isotherm at 77 K. Research purity krypton was obtained from the Matheson Tri-Gas Company. The isotherm was constructed by placing a soot-coated glass tube in a custom-made glass flask with one inlet. The glass tube was coated on the inside with either Type A or B soot and possessed the same internal radius (0.8 cm) but only half the length (10 cm) of the tubes used in the uptake experiments. The geometric surface area of the soot inside the tube was 50.24 cm^2.

To effectively degas the soot sample, a heating tape maintained a temperature of ∼473 K for a minimum of 1 h under vacuum in the flask. Following heating, a period of approximately 20 min was used to allow cooling under vacuum. The flask was submerged in liquid nitrogen so the soot surface was maintained at this temperature. Portions of Kr were subsequently added to the flask from a known initial volume while the pressure was monitored at each

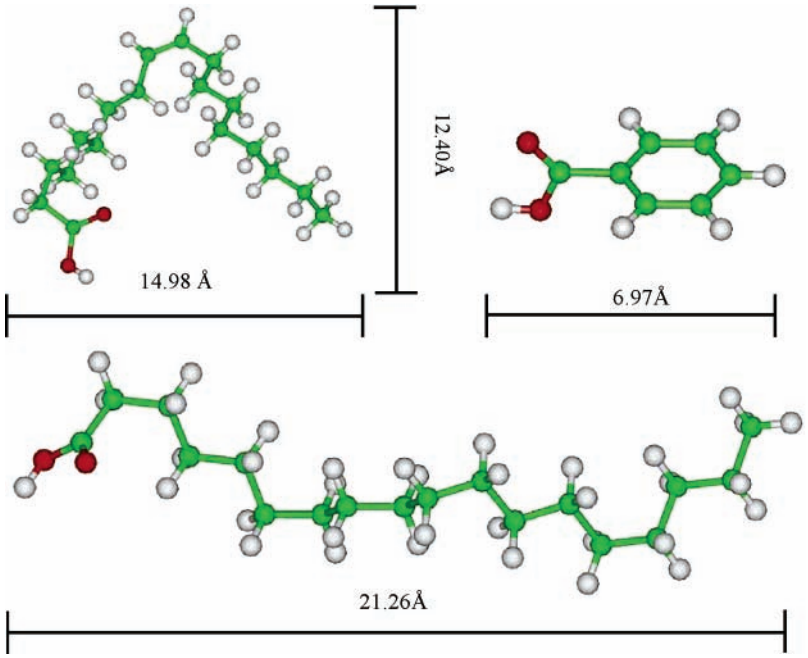

Figure 9. Theoretically optimized organic acid structures. Top left is oleic acid. Top right is benzoic acid. Bottom is steric acid.

step. A Varian Ceramicel CDG gauge barotron was used to measure pressure in our system. The pressure in the flask was corrected for thermal transpiration in the manner suggested by Rosenberg[61]

$$P = P_m\left[1 - \frac{0.490}{37.2D^2P_m{}^2 + 14.45DP_m + 1}\right] \quad (3)$$

where P is the corrected pressure in the flask, P_m is the pressure measured in the rest of the system by the barotron, and D is the diameter of the connection between the flask and the rest of the system. In this manner, it was possible to calculate the amount of Kr adsorbed by the soot surface from the known amount of krypton added, the known total volume of the system, and the change in pressures. The uptake of Kr and the surface area is described by the BET equation[62]

$$\frac{P}{V(P_0 - P)} = \frac{1}{V_mC} + \frac{P(C-1)}{V_mCP_0} \quad (4)$$

where P_0 is the saturation vapor pressure of the Kr, V is the adsorbed volume in units of cubic centimeters at standard temperature and pressure (STP), V_m is the volume of the monolayer capacity also at STP, and C is the dimensionless BET constant. Manipulation of this equation allows $P/[V(P_0 - P)]$ to be plotted against P/P_0, yielding a linear relationship.[63] From a linear fit of this plot, the BET constant and the monolayer capacity is extracted. The total surface area (SA_{BET}) of the soot measured is calculated by

$$SA_{BET} = V_mN_A\sigma_{Kr} \quad (5)$$

where V_m is the monolayer capacity converted to moles, N_A is Avogadro's number, and σ_{Kr} is the atomic cross-sectional area of Kr. The Kr saturation vapor pressure value used at 77 K was 2.49 Torr,[64] and the molecular area of Kr was taken to be 20.2 Å^2.[65] The saturation vapor pressure of supercooled liquid Kr was taken as P_0 because the Kr vapor pressure during experimentation was consistently found to be higher than the saturation vapor pressure of solid Kr (1.7 Torr) on soot samples.

3. Results and Discussion

3.1. Uptake of Organic Acids on Soot. Uptake measurements were performed by exposing a certain length of the soot to the organic acid vapor, while monitoring the organic acid signal using the ID-CIMS. For a few cases, the uptake of the organic acid on certain types of soot was found to be reversible. For example, in Figure 1 the maleic acid signal dropped upon exposure to a 20 cm length of Type B kerosene soot, but recovered near the level of the original signal. After returning the injector to the original position, the signal increased because of desorption of the organic acid. The adsorption curve was not symmetrical to that of desorption, but an estimation of the areas of the adsorption and desorption curves suggested desorption of much of the maleic acid taken up.

For most cases, the uptake was irreversible and adsorption to the solid soot was evident from the sharp decline in the organic acid signal. Figure 2 shows temporal profiles of phthalic acid as it exposed and later bypassed a 20 cm length of methane soot. The phthalic acid concentration in the gas phase dropped upon exposure to the soot and returned to approximately its original value after the exposure was terminated. The slightly higher signal after the injector was pushed in could be explained by some desorption of the organic acid or by a signal drift during the elapsed experimentation time. It was likely that desorption of organic acids could continue to take place with a slower rate after the termination of the exposure. At 900 s, the phthalic acid bubbler was bypassed to monitor the background for this species. The background level was similar to that of the phthalic acid being exposed to the methane soot, suggesting a nearly complete loss.

For the three monocarboxylic acids studied, most interactions were irreversible. The exceptions were benzoic acid on Type B propane and oleic acid on Type A kerosene soot. For benzoic acid, the uptake was reversible while oleic acid showed inconsistent uptake. Experiments were performed to obtain the

uptake coefficients for the monocarboxylic acids that showed clear irreversible uptake (Table 1). Figure 3a demonstrates the loss of benzoic acid as a function of the injector position when the injector was withdrawn at a 2.5 cm length interval. To prevent a significant saturation of the soot surfaces by the organic acid vapor, the injector was left at a single position for a shortest time possible. The decay followed the pseudo-first-order kinetics. The pseudo-first-order rate constant was determined from the slope of the linear least-square fit of the data shown in Figure 3b. The uptake coefficients were computed from the obtained pseudo-first-order rate constant.

The uptake of the monocarboxylic acids was observed to vary strongly with the exposure. For this reason, stepwise experiments were sequentially performed on one soot sample to measure the decrease in uptake coefficient over time. One uptake experiment lasted approximately 250−450 s, and after 6 experiments the soot had been exposed for roughly 35 min. Table 1 lists the average uptake coefficients for the experiments of each organic acid and soot type combination, illustrating the exposure dependence on the uptake coefficient. The mass listed for each combination was the average mass of the soot samples used for the experiments. In some cases, the uptake coefficient values on the sixth exposure had only half the value as those on the first exposure. For example, initial oleic acid loss to methane soot corresponded to an uptake coefficient of 0.95×10^{-2}, but the value decreased to 0.44×10^{-2} for the sixth exposure. We observed little dependence in the uptake coefficient on the gas-phase concentrations of the organic acids by varying the concentration by about a factor of 2−3 (using the temperature bath or altering flow rates). A trend was not evident from the table between the average mass used and range of uptake over exposures as might be expected. Figure 4 shows several uptake experiments of steric acid on Type A propane soot. The mass of soot used was different for each experiment, and no trend between soot mass and uptake was observed. These observations suggest that organic acid interaction with the soot was limited to the soot near the surface so the depth of the soot was irrelevant. It appeared that the soot physical or chemical makeup was more important than the amount when considering uptake.

The initial uptake coefficients of dicarboxylic acids measured in this study are summarized in Table 2 with the uptake coefficient values indicating irreversible uptake. The uptake behavior for maleic acid and Type A propane soot was rather inconsistent, so the uptake could not be considered fully reversible or fully irreversible. Using Type B propane soot under our conditions, no interaction or uptake was observed for oxalic acid or maleic acid and glutaric acid uptake was reversible. Also included in the table are the number of carbons in the organic acid carbon chain and the number of double bonds in that chain. Phthalic acid is an aromatic ring with two adjacent carboxylic acid groups bonded to the ring. The length of the carbon chain and its level of saturation may play a role in its ability to be taken up by soot. It has been suggested that for aromatic gases, the magnitude of adsorption enthalpies increases as conjugation and molecule complexity increases.[28] This trend has been linked to the vapor pressure of the organics and is possible due to the increasing ability to hydrogen bond and to have van der Waals interactions with the soot. These findings are supported by a recent theoretical study by Kubicki[29] that shows interaction between PAHs and soot is due mainly to $\pi-\pi$ system van der Waals forces. The calculations also show that larger and more aromatic molecules have a higher attraction to soot. In the present investigation, maleic acid had little or no irreversible uptake on soot while the other organic acids did show at least some irreversible uptake. Maleic acid was one of two carboxylic acids, omitting the cyclic compounds, which had a double bond in its carbon chain. The other was oleic, which also had relatively long sections of saturated carbon chain. Previous findings suggested that the double bond in maleic acid should contribute to interaction with the soot surface.[28,29] It is plausible that the carbon−carbon double bond and cis carboxylic acid group orientation in maleic acid may limit the interaction of the oxygenated functional group with the soot surface or facilitate more reversible characteristics. No gas-phase reaction products were detected during uptake experiments, and therefore it was not believed that organic acid molecules were reacting or disassociating on the soot surface and then re-entering the gas phase.

The observation of oxalic and glutaric acids interacting with soot irreversibly suggested that carboxylic acid groups were interacting with the soot carbon structure. These findings indicate that van der Waals interactions in steric acid and also $\pi-\pi$ system van der Waals forces in oleic acid and benzoic acid might contribute to uptake. More likely, both the carbon systems as well as oxygenated functional groups were involved in binding. For the cases such as benzoic acid on Type B propane soot and oleic acid on Type A kerosene soot, reversible interactions of the carbon system may dominate over irreversible mechanisms associated with oxygenated groups. Further investigation is necessary to elucidate how oxygenated functional groups facilitate irreversible uptake as compared to reversible interactions associated with nonoxygenated hydrocarbons.

Except for maleic acid, the uptake tended to increase as the dicarboxylic acids increase in the carbon number. This was consistent with previous findings that larger or more aromatic molecules will be more attracted to soot.[28,29] The uptake values can also be compared between the mono and dicarboxylic acids. Dicarboxylic acid uptake in general was on the same order of monocarboxylic acid uptake on methane soot or that of benzoic acid. No striking difference was noticed in the initial uptake between the two most structurally similar mono and dicarboxylic acids, i.e., benzoic, and phthalic (the two compounds differ only for one carboxylic group). The uptake behavior of the two compounds was similar on methane and Type A propane. However, phthalic acid was irreversibly taken up by Type B propane soot while benzoic acid was not, and benzoic acid was significantly higher on kerosene soot for both types than phthalic. If oxygenated functional groups aid in irreversible uptake, this might help explain the difference on Type A propane, but not on the kerosene samples.

3.2. Effect of Physical Properties on Uptake. FTIR and ATR-FTIR spectroscopy was employed to investigate functional groups that the ∼10% soot mass oxygen and hydrogen may constitute. FTIR was allowed to probe the bulk of the soot samples because IR light was shone though the soot mass deposited on the ZnSe disk. ATR was designed to allow interaction of the IR light with only the first few micrometers of the subject's surface. Assuming the internal surface area of the soot was of similar chemical composition to the external surface area, the ATR method was more applicable to the present study because the uptake of organic acids on soot was probably limited to surface interactions.

The investigation of bulk soot absorption did not indicate a significant amount of functionality. Figure 5a shows absorbance of propane soot over the wavelengths of 5000 to 750 cm^{-1}. The upper three spectra represent Type A soot and the bottom two spectra correspond to Type B. The baselines are not

TABLE 3: Summary of BET Measurements of Soot Surface Areas

methane

experiment	surface area[a]	soot mass[b]
1	174.85	3.7
2	112.42	8.3
3	114.41	9.4
4	160.24	5.0
5	108.10	18.0
average	134.00 ± 31.13[c]	8.9

propane

Type A			Type B		
experiment	surface area	soot mass	experiment	surface area	soot mass
1	56.29	18.9	1	150.63	18.3
2	106.04	24.3	2	166.61	15.4
3	93.00	36.4	3	148.15	16.4
4	58.47	41.9	4	122.42	16.1
average	78.45 ± 24.92	30.4	average	146.95 ± 18.29	16.5

kerosene

Type A			Type B		
experiment	surface area	soot mass	experiment	surface area	soot mass
1	75.26	16.9	1	98.30	14.4
2	68.93	69.0	2	92.75	19.1
3	81.40	63.6	3	133.25	5.6
4	48.69	190.2	4	97.51	28.9
5	58.58	115.9	5	93.67	59.6
6	n/a	n/a	6	112.05	44.5
average	66.57 ± 13.08	91.1	average	105.50 ± 18.70	28.7

[a] Surface areas are in units of $m^2\ g^{-1}$. [b] Soot masses are in units of mg. [c] Error corresponds to unbiased second standard deviation (2σ).

corrected and the spectra are shifted for clarity. The slopes are slightly different for each case, likely due to variations in soot thickness, but are very similar otherwise. No clear functionality was apparent in any of the FTIR spectra. For soot investigation with ATR spectroscopy, very similar spectra were obtained. Figure 5b depicts Type B (top) and Type A (bottom) kerosene soot ATR spectra. Again, the baselines are uncorrected and are shifted for clarity. As in the case of FTIR spectra, slopes vary slightly but absorbance over the wavenumbers studied are very similar between Types A and B soot as well as between different types of soot. These methods did not show noticeable functional groups formed from oxygen in soot that may facilitate uptake and any chemical difference between soot produced from different fuels. From the investigation by FTIR and ATR-FTIR, we concluded that no noticeable chemical difference existed between Types A and B soot.

To further characterize the physical properties of the soot as they pertain to organic acid uptake, we measured the surface area of each type of soot used for uptake experiments. The BET isotherm used to measure this quantity is similar to the Langmuir isotherm, but is able to account for multilayer adsorption of the condensing gas. Figure 6a shows an example of a BET isotherm. Notice that the large Kr uptake without any significant P/P_0 change at the beginning and end of the isotherm indicating a Type 2 Isotherm.[66] As described in the experimental section, the linear form of the BET equation can be plotted as P/P_0 versus $P/[V(P_0 - P)]$. An example of this can be seen in Figure 6b for the case of Kr adsorption on Type B kerosene soot. The values determined by this method are presented in Table 3. For methane, a single set of values was listed because soot deposition was not efficient enough if Type B soot was collected. For the other two types of soot, the effect of Type A versus Type B soot was apparent. The BET constants found for the two propane cases are 70 for Type B soot and 114 for Type A soot. It is apparent from the table that Type B propane soot has a larger surface area density of 146 $m^2\ g^{-1}$ than Type A propane soot of 78 $m^2\ g^{-1}$. The same trend was found for kerosene soot, but the difference was smaller. Type B kerosene soot shows an average of 105 $m^2\ g^{-1}$, while Type A kerosene soot has the lowest surface area with 66 $m^2\ g^{-1}$. The averaged BET constants for Types A and B kerosene soot were 168 and 106, respectively. From the comparison of these two fuels, it appeared that Type A soot preparation had a tendency to decrease the surface area of soot. Methane soot deposited in the Type A manner averaged a surface area of 134 $m^2\ g^{-1}$ and had a BET constant of 32. Another trend from Table 3 was the general increasing surface area per mass with decreasing amount of soot used for the experiment. This was likely due to lower soot levels being increasingly less likely to be probed by Kr molecules. It has been reported that that at a certain mass, the amount of surface area did not further increase with the soot amount from BET investigations of *n*-hexane soot.[35] The surface area measured here for methane was higher than the values of up to 50 $m^2\ g^{-1}$ or more reported by Tesner and Shurupov.[67] Our conditions were quite different from their heat-induced pyrolysis and soot collection method. The value of kerosene BET surface area reported by Choi and Leu[39] of 91 $m^2\ g^{-1}$ fell between the values reported here for Types A and B kerosene soot. Ferry et al.[23] reported a BET surface area measured with Kr for kerosene soot to be 44 $m^2\ g^{-1}$. The soot amount used was over three times the average used during our experiments, which might help explain the difference. On the other hand, BET surface area found by a commercial instrument for kerosene was reported as 120 ± 20 $m^2\ g^{-1}$ by Lelièvre et al.[36] We are not aware of a published value for propane soot surface area. Pore volume analysis was not performed because organic acids were not expected to accumulate enough to fill internal pores. In addition, it has been suggested that the pore volume analysis is largely applicable to Type IV isotherms, and its applicability to Type II isotherms and their hysteresis loops is question.[62]

The actual soot surface area was probably much larger than the geometric surface area assumed when determining the uptake

coefficient. Using the soot surface areas listed in Table 3, the possible implication of increased surface area on uptake coefficients can be estimated. Total soot surface areas of the higher soot masses used in this study can have surface areas higher than the geometric surface area. Correspondingly, the uptake coefficients can be lower if organic acids reached every possible square centimeter. On the other hand, the soot surfaces had many layers of packing, and the organic vapor likely only sampled a limited portion of micropores. It was also plausible that the sticky nature of organic acids made diffusion into internal layers difficult and only the upper layers were reached by organic molecules, as proposed for HNO_3 uptake on kerosene soot.[39] Hence, organic acid diffusion into the internal surface would be slower than predicted by simplified diffusion models. The effect of internal surface areas of soot on the uptake coefficient of organic acids requires further experimental and theoretical studies. Nevertheless, the present uptake coefficients represent an upper limit if the BET surface needs to be taken into account.

The effect of soot preparation, Type A versus Type B, on uptake coefficients can be further considered. The largest effect in the uptake coefficient between the two soot types in Table 1 corresponded to the case of propane soot. For each of the monocarboxylic acids, the Type A soot showed consistently higher initial uptake over Type B soot. The uptake of steric acid on Type A soot, while still higher, was relatively close to that on Type B soot for the first few measurements, but Figure 7 shows latter uptake was clearly higher for Type A soot. The same trend was observed in Table 2: the uptake was greater on Type A propane soot than Type B for the dicarboxylic acid. It is possible that Type B soot with a higher total surface area would be able to accommodate greater uptake and the higher average mass used in propane samples had an affect on the uptake. Kerosene soot did not show noticeable differences between Types A and B soot for monocarboxylic acids or dicarboxylic acids. While phthalic acid did have larger uptake on Type A kerosene soot than Type B, the error associated with Type A soot could indicate phthalic acid uptake was similar for both soot types.

Another phenomenon worth consideration is the variability of the averaged uptake coefficients over exposure time length. For most monocarboxylic acid/soot combinations, the uncertainty in the uptake coefficient was significantly less for the sixth exposure than for the first. In many cases, the error decreased with each exposure. This is apparent in Table 1 but one example is graphically illustrated in Figure 8 for steric acid uptake on methane soot. There was no correlation between average soot mass and decreasing variability, but there was for soot Type and organic acid. Most of the combinations that did not follow this trend involved benzoic acid, kerosene soot, and soot of Type B. On the other hand, the factors that appeared to facilitate this trend were steric acid involvement, propane soot, and Type A soot. The relatively larger surface area of propane and the effect that Type A preparation had on decreasing surface area likely explain why these two factors were associated with decreasing uptake variability with progressive exposures. Organic acids may block passages due to size issues or site favorability limiting organic acid uptake area to the geometric surface. More or less blockages during experimentation might have been facilitated by changes in flow reactor pressure, gas velocity, or radial injector position. Soot porosity and uptake site concentration may also have changed depending on soot deposition conditions. Factors such as room air turbulence, flame size, and fuel flow may have changed from deposition to deposition while trying to produce the sooting flame. With a more two-dimensional uptake field and loss of a degree of freedom, the variability between experiments should have diminished. While steric acid and oleic acid have the same number of carbons in the carbon chain, the cis double bond in oleic acid makes it slightly shorter (by 42%). Nevertheless, the interaction of the two molecules with soot substrate likely depended on their configuration on the soot surface. A related phenomenon has been observed by Kwon and Pignatello when studying benzene adsorption by charred maple wood shaving.[68] They found benzene adsorption at 293 K was slightly depressed after char was exposed to vegetable oil, but N_2 BET isotherms at 77 K showed a significant decrease in the internal surface area. Both observations were attributed to micropore throat blockage. Ferry et al. used transmission electron microscopy imaging and adsorption isotherms to determine the diameters of nanotube-like pores in kerosene soot.[23] They reported diameters of a few to several nanometers wide and a theoretical estimation of steric acid and oleic acid molecular length of 2.1 and 1.5 nm, respectively, putting these compounds at the lower end of this range. We have performed theoretical calculations using the GAUSSIAN 03 software package to investigate the molecular dimensions of organic acids. The level of density functional theory used in this study was Becke's three-parameter hybrid method. The LYP correction function was also considered giving (B3LYP) total theory. The mathematical restriction of the molecular orbitals, or basis set, used was a split valence-polarized basis set. The d and p orbital functions were added for a basis set of 6-31G(d,p) or 6-31G**. Optimized geometries of benzoic, steric, and oleic acids are depicted in Figure 9. Benzoic acid is the shortest of the monocarboxylic acids studied with a length of about 0.7 nm, while the length difference between steric acid and oleic acid is significant considering the only difference between their structures is merely one bond type. If steric acid was more likely to block internal soot passages because it is longer, this might explain why it was associated with decreasing uptake with increasing exposure.

TABLE 4: Estimated Organic Acid Coverage of Geometric Soot Surface[a]

			propane		kerosene	
acid	conc[b]	methane	Type B	Type A	Type B	Type A
benzoic	1×10^{13}	3	n/a	11	16	20
oleic	8×10^{12}	54	188	158	86	n/a
steric	5×10^{11}	2	4	3	9	3

[a] Coverage given as percentage. [b]Estimated concentration in flow tube given in molecules cm^{-3}

To further assess the location of organic acid uptake and the extent to which organic acids partition to the internal surface area, we estimated the amount of monocarboxylic acids taken up by the different soot types (Table 4). Using the organic acid concentrations and experimental signal levels, the number of organic acid molecules lost to the soot surface was determined to estimate the monolayer surface area that the organic acids occupy. Coverage of total BET soot surface areas was very small (0.001−0.04%) but if geometric surface area coverage was considered, the occupied space would have been more significant. The estimated geometric surface area coverage is also given in Table 4. The benzoic acid value of 3−20% was too low to implicate uptake location, but the large oleic acid values, especially those over 100%, confirmed that this species (if not all) was able to adsorb to soot below the surface level. The benzoic acid coverage was likely related to its higher volatility and lower uptake coefficient. Steric acid geometric surface area coverage was on the low side with only a few percent, but this

was likely due to its low concentration in the flow tube. The low coverage of steric acid on soot surfaces appeared to conflict with the assessment that this molecule might be abundant enough on soot surfaces to block pore throats and thereby lower uptake variability. While the surface coverage presented in Table 4 corresponds only to estimations and could not rule out pore blockage, the results suggest that uptake variability in the case of steric acid depended more on favorable site conditions and less on pore size for blockage. To assess soot aging by organic acids in the atmosphere requires knowledge of the available atmospheric particulate internal surface area and partial vapor pressures of the organic acids in the global atmosphere. To the best of our knowledge, there is little information on these quantities.

4. Conclusions

In this work, we have presented measurements of heterogeneous uptake of organic acids on Type A methane soot and both Types A and B propane and kerosene soot at 296 K. Most carboxylic acids interacted with the different soot types irreversibly, while a few uptakes were reversible. For the carboxylic acids that showed irreversible uptake, the uptake coefficient (γ) was experimentally determined. Monocarboxylic acid uptake coefficients were collected for a series of exposures to evaluate the "aging" effect. The uptake coefficient was found to vary depending on the fuel used to produce the soot and other factors. Chemical composition and surface areas of the soot surfaces were investigated to help understand factors affecting uptake.

Uptake of organic molecules on soot has been known to be driven by hydrogen bonding and van der Waals forces. Special $\pi - \pi$ interactions between unsaturated organic bonds and aromatic soot continuum have recently been studied. Previous experimental and theoretical results of PAHs show that these interactions are reversible so it is unclear if and how these attractive forces are alone causing the irreversible uptake observed in our experiments.[28,29] Small dicarboxylic acids exhibited uptake on the same order as monocarboxylic acids, likely indicating that carboxylic acid groups are participating in binding to soot surfaces. A recent soot structure investigation has shown that soot nanostructure may be less uniform than graphite;[69] the evidence shows small ring moieties that have higher hydrogen content and more molecular-like character. It may be possible that these molecules within the soot superstructure also have functionality conducive to interaction with carboxylic acids. More investigation is needed to determine the role oxygenated functional groups play in VOC adsorption to soot surfaces.

The uptake coefficients for monocarboxylic acids on a variety of soot types measured in this study ranged from 1.4×10^{-3} to 1.0×10^{-1}, and the uptake coefficient in the range of 9.0×10^{-4} to 7.7×10^{-3} was found for dicarboxylic acids. The uptake coefficient for monocarboxylic acids changed due to repeated exposures to the same soot sample. The uptake coefficients generally decreased by half after six exposures, but more dramatic reductions were also observed. For monocarboxylic acids, the propane and kerosene fuels used to produce soot showed comparable uptake of organic acids, but methane soot showed consistently lower uptake coefficients. Oleic acid and steric acid had medium to high uptake in most cases while benzoic acid uptake was lower on each type of soot. Maleic acid exhibited little or no irreversible uptake, but other dicarboxylic acids were lost to soot surfaces in roughly the same magnitude as monocarboxylic acids. The manner in which the soot was deposited also affected the uptake coefficients. Type A soot tended to facilitate slightly larger uptakes than Type B soot, especially for propane.

To probe the effect chemical composition has on organic acid uptake, FTIR and ATR spectroscopy were employed. All soot exhibited similar absorption spectra suggesting functionality of soot was effectively nonexistent throughout the soot mass. Furthermore, no difference was observed between Types A and B soot by either of the two infrared methods. These results show another physical or chemical difference was accountable for variations in uptake. BET adsorption isotherms measuring the surface area of soot samples were in the range of 66−146 $m^2 g^{-1}$. Type B soot samples showed larger surface areas than their Type A counterparts. It is unclear why smaller surface areas would be conducive to greater uptake, although it is possible that soot formed in the Type A manner caused another structural difference at the molecular or soot monomer unit level between the two types of soot undetectable by our methods.

Further investigation is needed to clarify binding mechanisms between oxygenated hydrocarbons and soot as well as the effect of Type A soot has on soot substructure. The present results show that many organic acids have significant uptake interactions with common atmospheric soot. The interaction between organic acids and soot may have implications for cloud microphysical properties, human health, radiative forcing, and global climate through alteration of the hydroscopic and optical properties of freshly formed soot aerosols.

Acknowledgment. The authors are thankful to Sarah Brooks for the use of the ATR instrument. Support from the U.S. Department of Energy National Institute for Climate Change Research (NICCR), the Robert A. Welch Foundation (Grant A-1417), and NSF (ATM-0424885) is acknowledged. Two referees provided insightful reviews to improve the manuscript.

References and Notes

(1) Yu, H.; Kaufman, Y. J.; Chin, M.; Feingold, G.; Remer, L. A.; Anderson, T. L.; Balkanski, Y.; Bellouin, N.; Boucher, O.; Christopher, S.; DeCola, P.; Kahn, R.; Koch, D.; Loeb, N.; Reddy, M. S.; Schulz, M.; Takemura, T.; Zhou, M. *Atmos. Chem. Phys.* **2006**, *6*, 613−666.

(2) Lance, S.; Nenes, A.; Rissman, T. A. *J. Geophys. Res.* **2004**, *109*, D22208, doi:10/1029/2003JD003697.

(3) Houghton, J. T.; Intergovernmental Panel on Climate Change. Working Group I. In *Climate Change 2001: The Scientific Basis: Contribution of Working Group I to the Third Assessment Report of the Intergovernmental Panel on Climate Change*; Cambridge University Press: Cambridge, U.K., 2001.

(4) Zhang, R. Y.; Suh, I.; Zhao, J.; Zhang, D.; Fortner, E. C.; Tie, X. X.; Molina, L. T.; Molina, M. J. *Science* **2004**, *304*, 1487−1490.

(5) Bond, T. C.; Streets, D. G.; Yarber, K. F.; Nelson, S. M.; Woo, J. H.; Klimont, Z. *J. Geophys. Res.* **2004**, *109*, D14203, doi:10.1029/2003jd003697.

(6) Penner, J. E.; Eddleman, H.; Novakov, T. *Atmos. Environ.* **1993**, *27*, 1277−1295.

(7) Schultz, E. *Atmos. Environ.* **1993**, *27*, 1241−1249.

(8) Gray, H. A.; Cass, G. R.; Huntzicker, J. J.; Heyerdahl, E. K.; Rau, J. A. *Sci. Total. Environ.* **1984**, *36*, 17−25.

(9) Kaneyasu, N.; Murayama, S. *J. Geophys. Res.* **2000**, *105*, 19881−19890.

(10) Finlayson-Pitts, B. J.; Pitts, J. N. *Chemistry of the Upper and Lower Atmosphere : Theory, Experiments, and Applications*; Academic: San Diego, CA, 2000.

(11) Lawrence, J.; Koutrakis, P. *J. Geophys. Res.* **1996**, *101*, 9171−9184.

(12) Peng, C.; Chan, M. N.; Chan, C. K. *Environ. Sci. Technol.* **2001**, *35*, 4495−4501.

(13) Yao, X. H.; Fang, M.; Chan, C. K. *Atmos. Environ.* **2002**, *36*, 2099−2107.

(14) Rogge, W. F.; Hildemann, L. M.; Mazurek, M. A.; Cass, G. R.; Simonelt, B. R. T. *Environ. Sci. Technol.* **1991**, *25*, 1112−1125.

(15) Rogge, W. F.; Hildemann, L. M.; Mazurek, M. A.; Cass, G. R.; Simoneit, B. R. T. *Environ. Sci. Technol.* **1993**, *27*, 2700−2711.

(16) Tervahattu, H.; Hartonen, K.; Kerminen, V. M.; Kupiainen, K.; Aarnio, P.; Koskentalo, T.; Tuck, A. F.; Vaida, V. *J. Geophys. Res.* **2002**, *107*, D16, doi:10.1029/2001JD001403.
(17) Ellison, G. B.; Tuck, A. F.; Vaida, V. *J. Geophys. Res.* **1999**, *104*, 11633−11641.
(18) Matsumoto, K.; Kawamura, K.; Uchida, M.; Shibata, Y.; Yoneda, M. *Geophys. Res. Lett.* **2001**, *28*, 4587−4590.
(19) Fang, J. S. E.; Kawamura, K.; Ishimura, Y.; Matsumoto, K. *Environ. Sci. Technol.* **2002**, *36*, 2598−2604.
(20) Mochida, M.; Kitamori, Y.; Kawamura, K.; Nojiri, Y.; Suzuki, K. *J. Geophys. Res.* **2002**, *107*, D17, doi:10.1029/2001JD001278.
(21) Mansurov, Z. A. *Combust. Explos. Shock Waves* **2005**, *41*, 727−744.
(22) Seinfeld, J. H.; Pandis, S. N. *Atmospheric chEmistry and Physics: From Air Pollution to Climate Change*; Wiley: New York, 1998.
(23) Ferry, D.; Suzanne, J.; Nitsche, S.; Popovitcheva, O. B.; Shonija, N. K. *J. Geophys. Res.* **2002**, *107*, D23, doi:10.1029/2002JD002459.
(24) Stanmore, B. R.; Brilhac, J. F.; Gilot, P. *Carbon* **2001**, *39*, 2247−2268.
(25) Alcala-Jornod, C.; Rossi, M. J. *J. Phys. Chem. A* **2004**, *108*, 10667−10680.
(26) Horvath, H. *Atmos. Environ.* **1993**, *27*, 293−317.
(27) Schnaiter, M.; Horvath, H.; Mohler, O.; Naumann, K. H.; Saathoff, H.; Schock, O. W. *J. Aerosol Sci.* **2003**, *34*, 1421−1444.
(28) Aubin, D. G.; Abbatt, J. P. *Environ. Sci. Technol.* **2006**, *40*, 179−187.
(29) Kubicki, J. D. *Environ. Sci. Technol.* **2006**, *40*, 2298−2303.
(30) Nguyen, T. H.; Ball, W. P. *Environ. Sci. Technol.* **2006**, *40*, 2958−2964.
(31) Alcala-Jornod, C.; van den Bergh, H.; Rossi, M. J. *Phys. Chem. Chem. Phys.* **2000**, *2*, 5584−5593.
(32) Zhang, D.; Zhang, R. Y. *Environ. Sci. Technol.* **2005**, *39*, 5722−5728.
(33) Stier, P.; Seinfeld, J. H.; Kinne, S.; Feichter, J.; Boucher, O. *J. Geophys. Res.* **2006**, *111*, D18, doi:10.1029/2006JD007147.
(34) Suzanne, J.; Ferry, D.; Popovitcheva, O.; Shonija, N. K. *Can. J. Phys.* **2003**, *81*, 423−429.
(35) Aubin, D. G.; Abbatt, J. P. *J. Phys. Chem. A* **2003**, *107*, 11030−11037.
(36) Lelievre, S.; Bedjanian, Y.; Pouvesle, N.; Delfau, J. L.; Vovelle, C.; Le Bras, G. *Phys. Chem. Chem. Phys.* **2004**, *6*, 1181−1191.
(37) Longfellow, C. A.; Ravishankara, A. R.; Hanson, D. R. *J. Geophys. Res.* **2000**, *105*, 24345−24350.
(38) Seisel, S.; Pashkova, A.; Lian, Y.; Zellner, R. *Faraday Discuss.* **2005**, *130*, 437−451.
(39) Choi, W.; Leu, M. T. *J. Phys. Chem. A* **1998**, *102*, 7618−7630.
(40) Kirchner, U.; Scheer, V.; Vogt, R. *J. Phys. Chem. A* **2000**, *104*, 8908−8915.
(41) Prince, A. P.; Wade, J. L.; Grassian, V. H.; Kleiber, P. D.; Young, M. A. *Atmos. Environ.* **2002**, *36*, 5729−5740.
(42) Longfellow, C. A.; Ravishankara, A. R.; Hanson, D. R. *J. Geophys. Res.* **1999**, *104*, 13833−13840.
(43) Al-Abadleh, H. A.; Grassian, V. H. *J. Phys. Chem. A* **2000**, *104*, 11926−11933.
(44) Korfmacher, W. A.; Wehry, E. L.; Mamantov, G.; Natusch, D. F. S. *Environ. Sci. Technol.* **1980**, *14*, 1094−1099.
(45) Yang, K.; Zhu, L. Z.; Xing, B. S. *Environ. Sci. Technol.* **2006**, *40*, 1855−1861.
(46) Zhu, D. Q.; Kwon, S.; Pignatello, J. J. *Environ. Sci. Technol.* **2005**, *39*, 3990−3998.
(47) Mikhailov, E. F.; Vlasenko, S. S.; Podgorny, I. A.; Ramanathan, V.; Corrigan, C. E. *J. Geophys. Res.* **2006**, *111*, D7, doi:10.1029/2005JD006389.
(48) Zhao, J.; Levitt, N. P.; Zhang, R. Y. *Geophys. Res. Lett.* **2005**, *32*, L09802, doi:10.1029/2004GL022200.
(49) Levitt, N. P.; Zhao, J.; Zhang, R. Y. *J. Phys. Chem. A* **2006**, *110*, 13215−13220.
(50) Zhao, J.; Levitt, N. P.; Zhang, R. Y.; Chen, J. M. *Environ. Sci. Technol.* **2006**, *40*, 7682−7687.
(51) Fortner, E. C.; Zhao, J.; Zhang, R. Y. *Anal. Chem.* **2004**, *76*, 5436−5440.
(52) Zhao, J.; Zhang, R. Y.; Fortner, E. C.; North, S. W. *J. Am. Chem. Soc.* **2004**, *126*, 2686−2687.
(53) Zhao, J.; Zhang, R. Y.; Misawa, K.; Shibuya, K. *J. Photochem. Photobiol. A* **2005**, *176*, 199−207.
(54) Keyser, L. F.; Moore, S. B.; Leu, M. T. *J. Phys. Chem.* **1991**, *95*, 5496−5502.
(55) Zhang, R. Y.; Jayne, J. T.; Molina, M. J. *J. Phys. Chem.* **1994**, *98*, 867−874.
(56) Zhang, R. Y.; Leu, M. T.; Keyser, L. F. *J. Phys. Chem.* **1994**, *98*, 13563−13574.
(57) Brown, R. L. *J. Res. Natl. Bur. Stand. (U.S.)* **1978**, *83*, 1−8.
(58) Fuller, E. N.; Schettle, Pd.; Giddings, J. C. *Ind. Eng. Chem.* **1966**, *58*, 19−&.
(59) Marrero, T. R.; Luecke, R. H. *AIChE J.* **1996**, *42*, 2365−2368.
(60) Brunauer, S.; Emmett, P. H.; Teller, E. *J. Am. Chem. Soc.* **1938**, *60*, 309−319.
(61) Rosenberg, A. J. *J. Am. Chem. Soc.* **1956**, *78*, 2929−2934.
(62) Gregg, S. J.; Sing, K. S. W. *Adsorption, Surface Area, and Porosity*, 2nd ed.; Academic Press: London, 1982.
(63) Sing, K. S. W.; Everett, D. H.; Haul, R. A. W.; Moscou, L.; Pierotti, R. A.; Rouquerol, J.; Siemieniewska, T. *Pure Appl. Chem.* **1985**, *57*, 603−619.
(64) Keyser, L. F.; Leu, M. T. *J. Colloid Interface Sci.* **1993**, *155*, 137−145.
(65) Zhang, R. Y.; Leu, M. T.; Keyser, L. F. *J. Geophys. Res.* **1995**, *100*, 18845−18854.
(66) Brunauer, S.; Deming, L. S.; Deming, W. E.; Teller, E. *J. Am. Chem. Soc.* **1940**, *62*, 1723−1732.
(67) Tesner, P. A.; Shurupov, S. V. *Combust. Sci. Technol.* **1995**, *109*, 399−400.
(68) Kwon, S.; Pignatello, J. J. *Environ. Sci. Technol.* **2005**, *39*, 7932−7939.
(69) Kis, V. K.; Posfai, M.; Labar, J. L. *Atmos. Environ.* **2006**, *40*, 5533−5542.